JOURNAL OF MATERIALS SCIENCE 30 (1995) 4676–4683

The effect of load level on the mechanism of fatigue crack propagation in ABS

T. J. BOHATKA*, A. MOET
Department of Macromolecular Science, Case Western Reserve University, 10900 Euclid Avenue, Cleveland, OH 44106–7202, USA

The fatigue crack propagation (FCP) mechanism of an ABS was examined under tension–tension loading as a function of load level. The crack was always preceded by a damage zone consisting of assemblies of stress-whitened lines. Crack growth was predominantly through the root damage line, with occasional jumps into neighbouring lines. These jumps occurred most frequently in the medium load level test. Transmission electron microscopy (TEM) analyses showed the damage within the stress-whitened lines to consist of elongated, and occasionally ruptured, rubbery domains at the specimen surface, with the appearance of extensive crazes bridging their interstices toward the mid-thickness. The craze intensity (size and number) increased with decreasing load level. The crazes manifested themselves on the fracture surface as a patch morphology, which was increasingly pervasive with decreasing load level. In the rougher region that followed, ductile tearing of the matrix is believed to be promoted by rubber cavitation and the merging of crazes. Normal fatigue striations indicate crack advance by greater fractions of the damage zone length at higher load levels.

1. Introduction

The notable toughness of the ABS polymer makes it a prime candidate for several engineering applications demanding resistance to crack propagation. In a previous paper, we have examined the applicability of linear elastic fracture mechanics [1] while in a subsequent paper we determine the specific enthalpy of fracture using the crack layer theory [2]. To elucidate the material response in resistance to crack advance, it is necessary to define the detailed mechanisms contributing to crack tip plasticity. Although the fatigue mechanism in ABS has been studied from fractographic observations [3,4], little is known about the underlying submicroscopic damage events preceding rupture (formation of fracture surfaces). The latter phenomena have been explored under monotonic loading [5,6] and can only be indirectly related to the mechanisms of fatigue crack growth. Further, the above mentioned fractographic studies have been conducted on un-notched specimens, thus their results cannot be linked to fatigue lifetime components (i.e. crack initation, stable and unstable propagation).

Since the damage mechanism results from the interaction of the stress field with the microstructure of the material, it is worth taking a brief moment to review the structure of ABS. ABS is a two phase system having styrene acrylonitrile copolymer as the continuous phase with a dispersed phase of butadiene-derived rubber. Depending on the method of polymerization, the rubber particles may be solid, or of the occluded variety, which contain sub-inclusions of the glassy matrix. In many systems, the rubber particle is surrounded by a shell of grafted polymer, which serves to promote adhesion to the matrix. In ABS made by the mechanical blending of the butadiene and resin, the absence of this graft layer results in greatly reduced toughness [7, 8]. The size of the rubbery inclusions also plays a role in the resulting mechanism, and is a function of the polymerization conditions.

Fractographic analyses leave some questions as to the role played by crazing in the fatigue mechanism of ABS. For example, Sauer and Chen [3] have found that in balanced tension–compression loading at a maximum stress of 20.7 MPa and a frequency of 21 Hz, the fracture surface in the region of the discontinuous crack growth (DCG) bands reveals a drawn and somewhat fibrillar morphology that they identify as fractured ligaments of craze fibrils. In an examination of tension–tension fatigue at the slightly higher load level of 27.5 MPa and the same frequency, drawn fibrillar elements highly resembling those found in the tension–compression study were also found [4]. These structures, however, were not attributed to crazes and were more cautiously described as extensive plastic deformation. It seems that such ambiguity could be resolved by supplementing the fracture surface analysis with investigations into the microscopic details of the damage zone.

Detailed analyses of damage in thin film and bulk specimens of ABS subject to tensile loading imply that microstructural variables should play a role in the FCP mechanism. For example, these studies have

* Author to whom correspondence should be addressed.

0022–2461

found that variations in the size of the dispersed rubbery phases [5] as well as the molecular weight of the matrix [6] can produce behaviours ranging from crazing to a lack thereof. One study on thin films suggests that small rubber particles ($\sim$0.1 μm diameter) deform predominantly by cavitation, while larger particles ($\sim$1.5 μm) are more effective at nucleating crazes [5]. Lending further support to this is work done on bulk specimens containing small rubber particles ($\sim$0.5 μm), in which rubber cavitation was the dominant mode of deformation [9]. In another study, however, significant crazing was observed in bulk ABS specimens containing small rubber particles ($\sim$0.3 μm), when tested at about one-tenth the strain rate [6]. This underlines the fact that the damage mechanism is a product of both the material microstructure as well as the imposed loading conditions. Once crazes are formed, it appears that their growth is unaffected by small rubber particles. Larger particles, on the other hand, seem to inhibit craze growth with energy dissipating mechanism [5]. Work done on HIPS suggests that the ability of larger rubber particles to inhibit craze growth derives from their occluded nature [10].

In light of our previous report which has shown how different load levels can produce differences in FCP kinetics [1], this paper identifies the mechanistic origin of these differences and relates the various damage species within the plastic zone to the fractographic features.

2. Experimental procedure

2.1. Material

The ABS used in this study was in the form of injection-moulded plaques. Image analysis of TEM micrographs showed the percentage volume of the rubbery domains to be in the range of 30–40%. These domains are of the occluded variety, with diameters ranging from 0.3–1.2 μm and an average diameter of 0.75 μm. The acrylonitrile content is greater than 15%. Tensile testing at 25 °C and a strain rate of 25% min^{-1} determined the yield stress to be 46 MPa.

2.2. Fatigue testing

Specimens were cut from the injection-moulded plaques and machined into rectangular, SEN specimens of dimensions 25.4 × 3.3 mm with a gauge length of 102 mm. A 60° notch was then machined into the edge to a depth of 2.54 mm and then finished off with a razor blade to a total notch depth of 3.5 mm. The direction of crack propagation was perpendicular to the mould flow direction.

Fatigue testing was done using an MTS servohydraulic testing machine. The loading was tension–tension using a sinusoidal waveform with the R-ratio ($\sigma_{min}/\sigma_{max}$) maintained at 0.1. The frequency was kept low, at 1Hz, to avoid hysteretic heating. The maximum load level (σ_{max}) was the testing variable and was set at values of 5.0, 7.5, and 10.8 MPa, (11,16, and 23% of the yield stress, respectively). All tests were performed at a temperature of 25 °C. Throughout each test, the crack length was monitored with a travelling microscope.

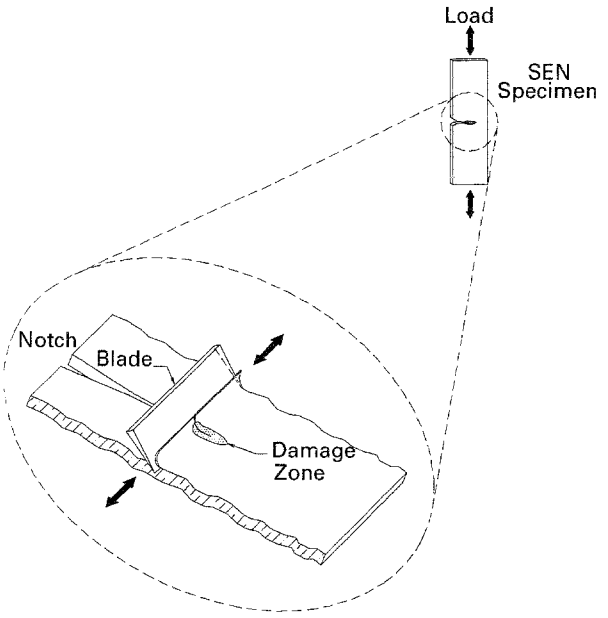

Figure 1 Illustration of sectioning method.

2.3. Microscopy

Each of the load levels tested was interrupted at various crack lengths and detailed microscopic analyses of the damage zones were performed. To obtain a profile of the damage through the thickness dimension, 60 μm thick sections were cut at − 40 °C as illustrated in Fig. 1. The sections were then placed on glass slides and photographed under transmitted light. The fracture surfaces of broken specimens were sputter-coated with gold and viewed using a Joel-840A scanning electron microscope.

TEM sample preparation was done according to the methods prescribed by Dillon and Bevis [6]. For each sample, a fresh glass knife with a nominal bevel angle of 45° was made using a GKM glass knife maker. An MT 6000-XL microtome was then used to cut 90nm thick sections, in the same orientation illustrated above (Fig. 1), at a cutting speed of 2 mm s^{-1}. All of the sections were taken from about the centre of the damage zone, just ahead of the crack tip. The sections were viewed using a Jeol JEM-100SX transmission electron microscope.

3. Results and discussion

Fig. 2 shows the fatigue lifetime plotted against the maximum stress (σ_{max}). As σ_{max} decreases, the fatigue lifetime expectedly increases. However, at the onset, a significant decrease in σ_{max} produces a minimal increase in lifetime. Beginning at $\sigma_{max} \cong 6$ MPa, however, minor decreases in σ_{max} produce significant increases in lifetime. The second regime has been identified with the conditions under which FCP approaches the long-term stability associated with service conditions. In the subsequent mechanistic analysis, we chose load conditions belonging to both the

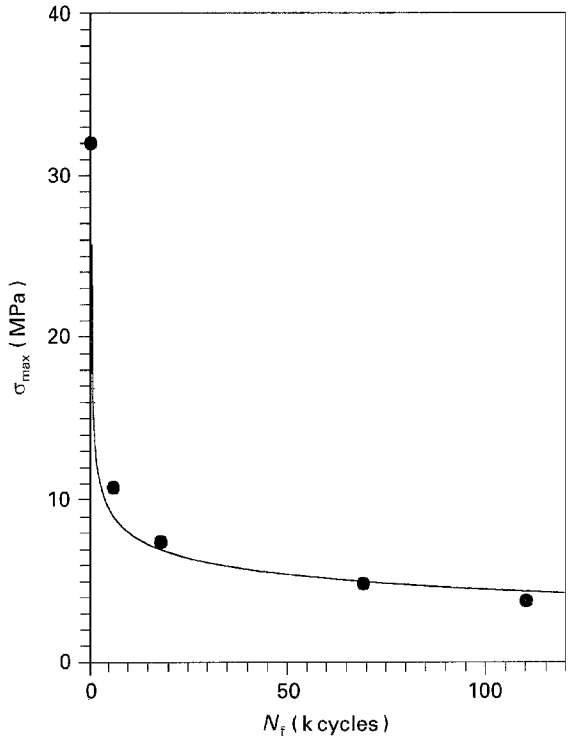

Figure 2 Notched S-N curve showing stabilization to an "endurance limit" as the load level is decreased.

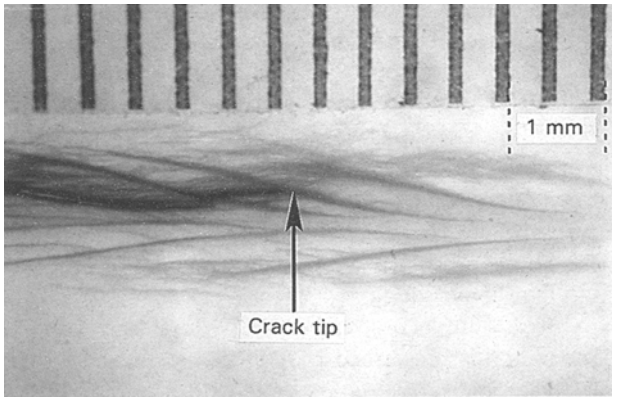

Figure 3 The crack tip and its accompanying zone of damage.

former regime (σ_{max} = 10.8 and 7.5 MPa), and the latter (σ_{max} = 5.0 MPa). The hierarchy of the damage mechanism will be examined on several complementary levels of scale within the damage zone and the fracture surface.

3.1. Evolution of the crack tip damage zone

3.1.1. Continuum Perspective

At all load levels tested, observation of the crack from the side view perspective of Fig. 1 revealed a zone of damaged material surrounding the crack tip (Fig. 3). Although the damage zone is comprised of a multitude of stress-whitened lines, they are assembled into the characteristic shape of a plane stress plastic zone. Sectioning into the mid-plane revealed that the damage zone size remains nearly the same as on the surface, though its boundary is somewhat less defined.

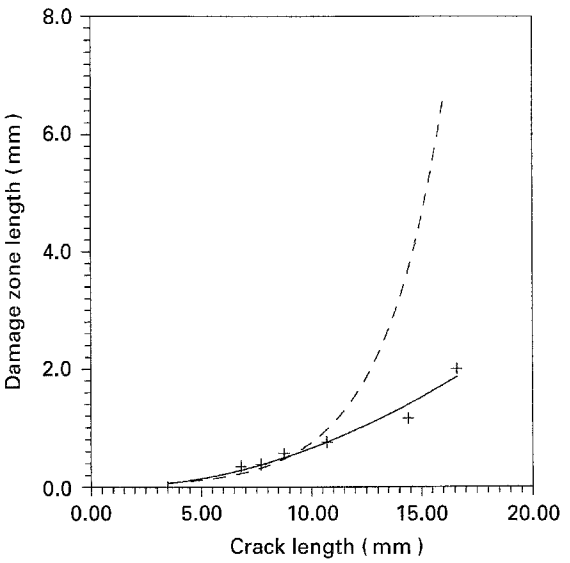

Figure 4 Typical relation between the measured (+) and Dugdale (–) damage zone lengths (σ_{max} = 5.0 MPa).

Given the linear character of the damage zone, the ability of the Dugdale model to describe the damage zone length is worth considering here. By virtue of the model, the maximum stress intensity factor (K_{max}) should dictate the damage zone length by

$$r_p = \frac{\pi}{8}\left(\frac{K_{max}}{\sigma_y}\right)^2 \quad (1)$$

where r_p is the damage zone length and σ_y is the yield stress.

As seen in Fig. 4, Equation 1 provides a close estimate of the damage zone length at low crack lengths, but deviates significantly at higher crack lengths. This is not surprising in light of the fact that the larger damage zones produced at higher crack lengths will militate against linear elasticity, and hence the validity of K. The fact that Equation 1 overestimates the damage zone length suggests that the damage effectively reduces the stress field ahead of the crack tip.

3.1.2. Rupture of the damage zone

As expected, the stress-whitened lines comprising the damage zone present planes of least resistance through which the crack grows. For the most part, the crack moves through the root damage plane, where the local stress magnitude is a maximum. Occasionally, however, the crack path is diverted into a neighbouring line of damage.

Fig. 5 is a transmitted light micrograph showing both a secondary internal crack about to jump into the plane of the primary crack plane, as well as the ridge formed as a result of a previous jump. The sequence of events that led to the formation of this ridge began with the formation of a small secondary internal crack just ahead of, and adjacent to, the crack tip. Once formed, the primary crack tip and the tip of the secondary internal crack closest to it, began to converge due to the complex interaction of their stress

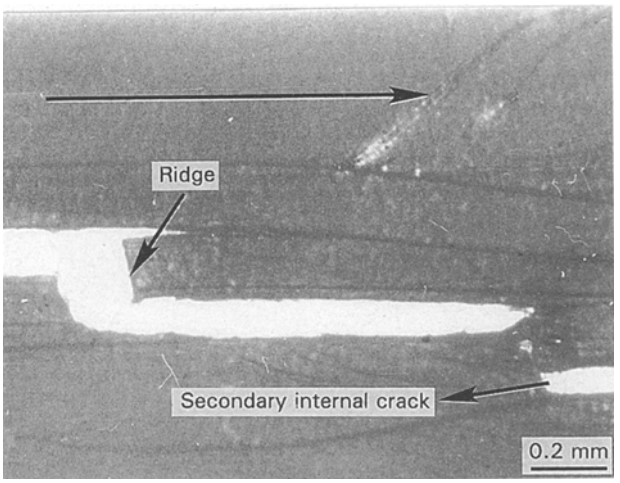

Figure 5 Transmitted light micrograph illustrating the mechanism of perturbations in the crack path.

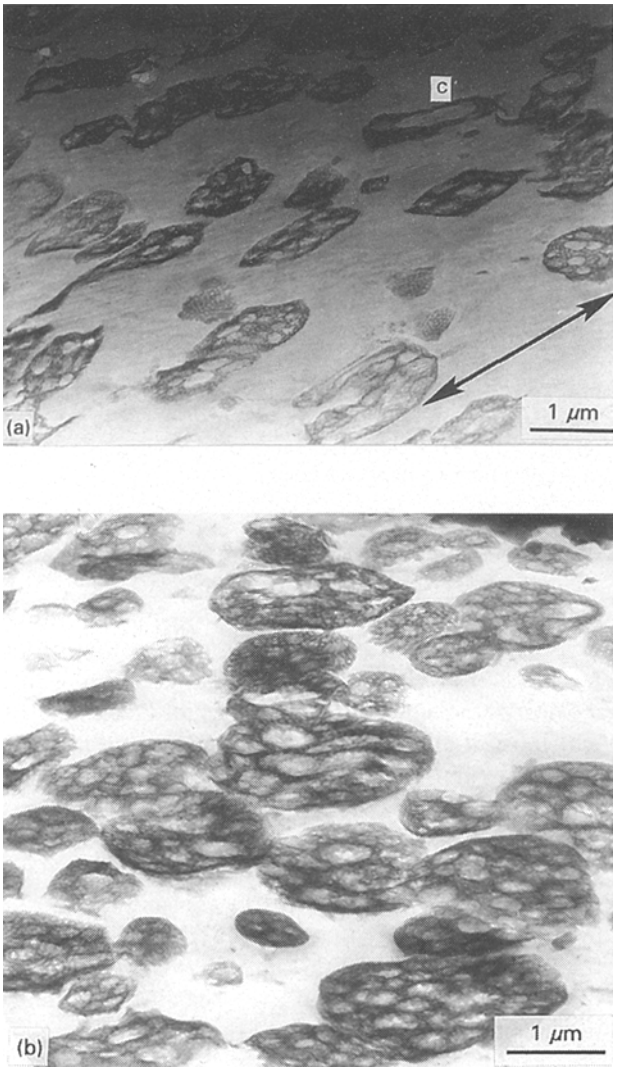

Figure 6 (a) TEM micrograph of the damage zone at the specimen surface, (C denotes site of possible rubber particle cavitation), (σ_{max} = 7.5 MPa and crack length is 10mm), and (b) undeformed specimen surface.

fields [11]. The material between the two cracks was then subject to intense bending. When this material became sufficiently weak, the secondary crack grew into the plane of the primary crack, leaving a characteristic ridge. The far end of the secondary crack then began to propagate as the new primary crack. Later, fractographic analysis will show that the secondary cracking associated with such ridge formation occurred most frequently at the medium load level tested (σ_{max} = 7.5 MPa).

Thus far, it has been shown that the stress-whitened lines dictate the crack path. The underlying microstructure of damage giving rise to such crack growth will now be examined. From Fig. 3, it is evident that the thickness of the stress-whitened lines is of the order of 130 μm and that they appear to be oriented perpendicular to the maximum principal stress trajectories [12]. For polystyrene, such damage entities were reported to be crazes having thicknesses of the order of 1 μm [13]. Whether or not this is true of the ABS studied here remains to be seen. For the moment, however, let it suffice to say that these lines reflect intensified damage planes dictated by the stress field ahead of the crack tip.

3.2. Microstructure of damage

3.2.1. Specimen surface

A TEM micrograph within a typical stress-whitened line as seen from the specimen surface is shown in Fig. 6a. Comparison with a similar section in the undeformed material is shown in Fig. 6b. It is noted that while Fig. 6a shows increased elongation of the rubbery domains due to the applied load, there is no evidence of crazing in the matrix as observed by Dillon and Bevis in monotonically fractured ABS [6]. This rubber domain elongation in the absence of crazing indicates shear yielding of the matrix.

It is believed that the observed stress whitening is produced by the deformation and subsequent orientation of the rubbery domains, as was the case in a rubber modified PVC [14]. In the ABS examined here, one also finds evidence of rubber cavitation ("C", Figs 6–8), though this was minimal. Such cavitation could also contribute to stress whitening [9].

3.2.2. Mid-thickness

The TEM micrographs of the mid-thickness damage zones taken at a crack length of 10 mm for both the low and high load levels are shown in Fig. 7a and b, respectively. The micrographs reveal not only elongation and occasional cavitation of the rubbery domains (C), but also crazing, which bridges their interstices. These crazes bear a remarkable resemblance to the crazes observed in ABS fractured under uniaxial tension observed by Dillon and Bevis [6]. In light of the previously discussed uncertainty regarding the role of crazing in the fatigue mechanism of ABS, the present work shows that crazing can play a significant role in the FCP mechanism of ABS.

Within the same damage zones of Fig. 7a and b, small regions of elongated, and occasionally cavitated rubbery domains (C) are found in the absence of crazing (Fig. 8a and b). This confirms that shear yielding of the matrix is also occurring at the specimen

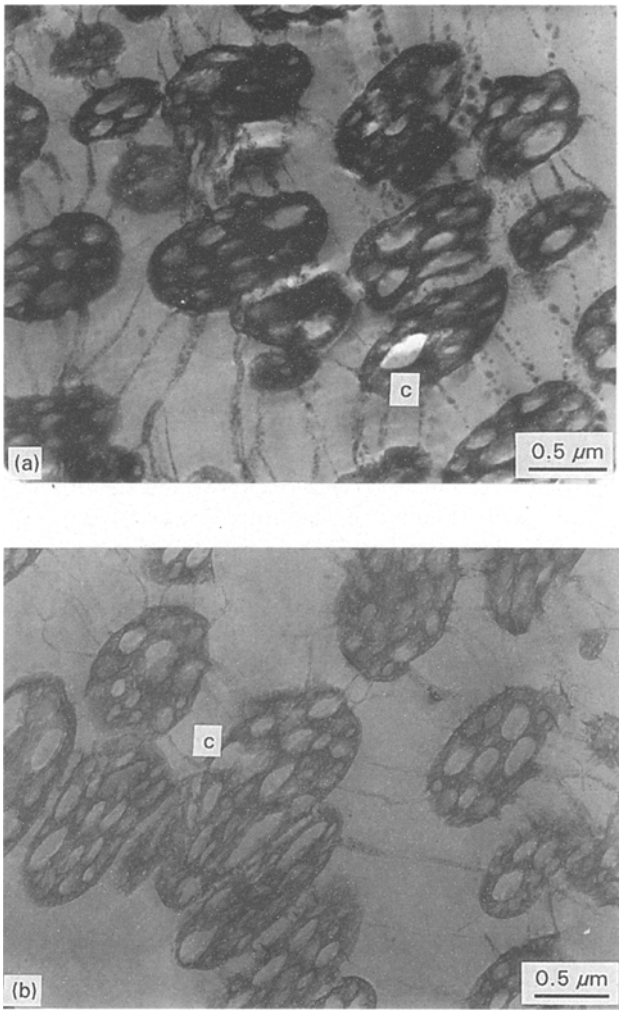

Figure 7 TEM micrographs of the damage zone at the mid-thickness plane for a crack length of 10 mm and (a) $\sigma_{max} = 5.0$ MPa, and (b) $\sigma_{max} = 10.8$ MPa; (C denotes site of possible rubber particle cavitation).

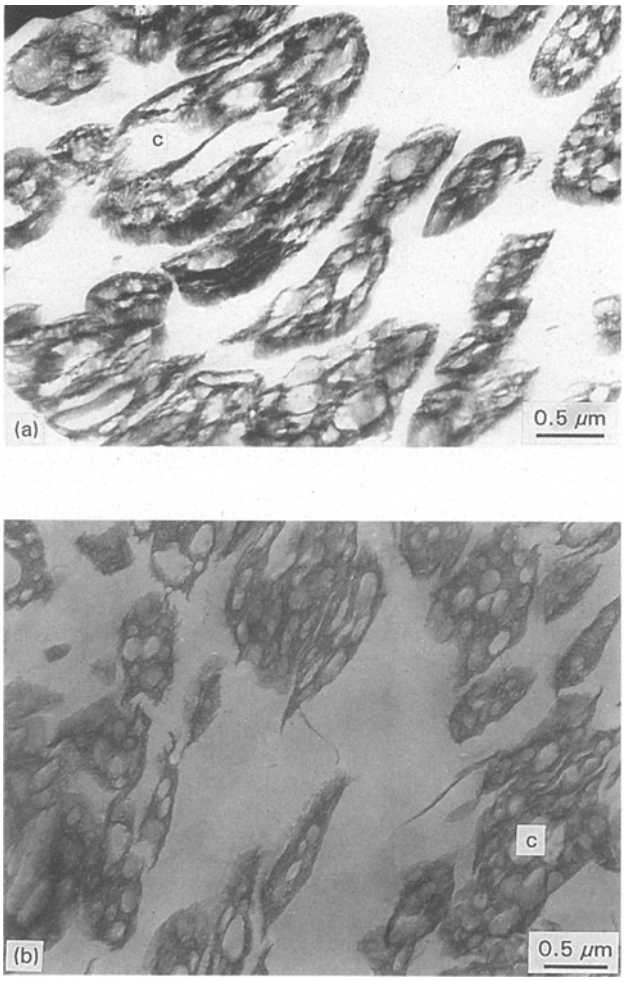

Figure 8 TEM micrographs of the damage zone at the mid-thickness plane for a crack length of 10 mm and (a) ($\sigma_{max} = 5.0$ MPa, and (b) $\sigma_{max} = 10.8$ MPa, showing the absence of crazes; (C denotes site of possible rubber particle cavitation).

mid-thickness. For the specimens examined, however, these regions were quite minimal. The average aspect ratio of the rubbery domains at both load levels for both the crazed (Fig. 7a and b) and uncrazed (Fig. 8a and b) regions of the mid-thickness damage zone are shown in Fig. 9. First, it is seen that in the uncrazed regions, both load levels show about the same amount of rubber domain elongation. In the crazed regions, however, elongation of the rubber domains is unexpectedly higher at the lower load level. This will later be explained by differences in craze development between the two load levels. At a given load level, the higher average aspect ratio of the rubbery domains in the uncrazed region as compared to that of the crazed region reflects the ability of crazes to localize deformation within their boundaries.

Crazing, a time-dependent phenomenon, should change intensity with changing load level. Table I shows the average craze width, W_c, average number of crazes per unit area, N_c/A, and the average volume fraction of crazes, ϕ_c, within a typical stress-whitened line just ahead of the crack tip as determined through image analysis [15]. Indeed, a larger volume fraction of crazing is found at the lower load level. This arises from both wider crazes (approximately four times), as well as a larger craze population density (N_c/A) . It is believed that craze nucleation and development would be promoted by the greater lifetime of the lower load level test. Further, a lower load level will produce a lower stress intensity factor over all crack lengths, which will in turn produce a smaller amount of strain per cycle (unit time). This lower strain rate will be more conducive to the molecular motions necessary for craze initiation and development. These findings are supported by other claims that the contribution of crazing in ABS increases with decreasing strain rate (i.e. strain per cycle in this case) [16]. Further supporting this is the work of Truss and Chadwick, who have indicated that at low strain rates, the amount of crazing increases with decreasing strain rate [17].

3.3 Fracture surface analysis

The fracture surfaces are shown in Fig. 10a–c. All the fracture surfaces exhibit contraction in the specimen thickness direction at the higher crack lengths. This thinning is indicative of shear yielding [18] and is more significant at higher load levels and crack lengths (higher K). All the load levels tested also exhibit a small, ill-defined initiation region characterized

TABLE I Average craze width ($\bar{w}_c$), average number of crazes per unit area, (N_c μm^{-2}), and volume fraction of crazes, (ϕ_c), for σ_{max} = 5.0 and 10.8 MPa (crack length = 10 mm) demonstrating more intense crazing at the lower load level

σ_{max} (MPa)	w_c (μm)	N_c μm^{-2}	ϕ_c
5.0	0.197	6.04	0.76
10.8	0.053	1.94	0.07

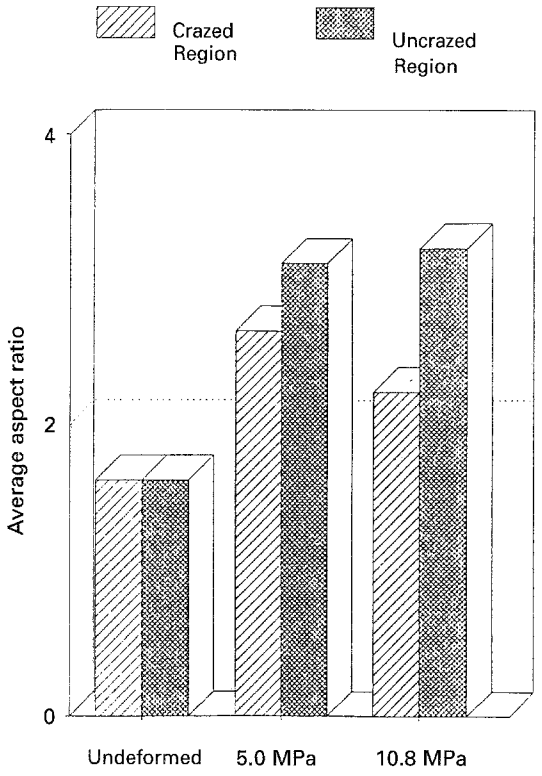

Figure 9 Average aspect ratio of the rubbery domains for the tests of σ_{max} = 5.0 and 10.8 MPa in both the crazed (▨) and uncrazed regions (■) of the damage zone at the specimen mid-thickness.

by a relatively smooth surface containing a minimal number of secondary cracks. Further, the DCG bands (D) characteristic of FCP are discernible in the last region of stable crack growth for all the load levels tested. The bands are then followed by a catastrophic region characterized by parabolic secondary cracks and level difference lines. Focusing on the region of stable crack propagation, where formation of the fracture surfaces is dictated by the development of damage within the plastic zone, the variations in the fracture surface features with changing load level will now be examined.

3.3.1. Secondary cracks

Analysis of the lowest load level (Fig. 10 c) indicates that the previously observed ridges at the specimen surface (i.e. Fig. 5) originate from deep within the specimen thickness. The point labelled R′ shows a typical ridge believed to be produced by the previously described growth of a secondary internal crack into the plane of the primary crack. When this ridge (R′) is viewed from a direction orthogonal to the fracture surface (Fig. 11), the morphology and size scale indicate that this is the same type of feature shown in Fig. 5. Looking back at the fracture surface (Fig. 10c), the fact that this ridge is angled toward the specimen surface in the direction of crack propagation indicates that the secondary crack originated near the specimen mid-thickness, just ahead of the primary crack front.

It is noted here that such impingement of primary and secondary cracks is not always manifested at the side view. Indeed, preliminary side view observations showed the greatest abundance of these ridges at the lowest load level. The fracture surfaces, however, show the most crack impingement at the test of σ_{max} = 7.5 MPa. This apparent discrepancy is explained as follows. For the test of σ_{max} = 7.5 MPa, the level

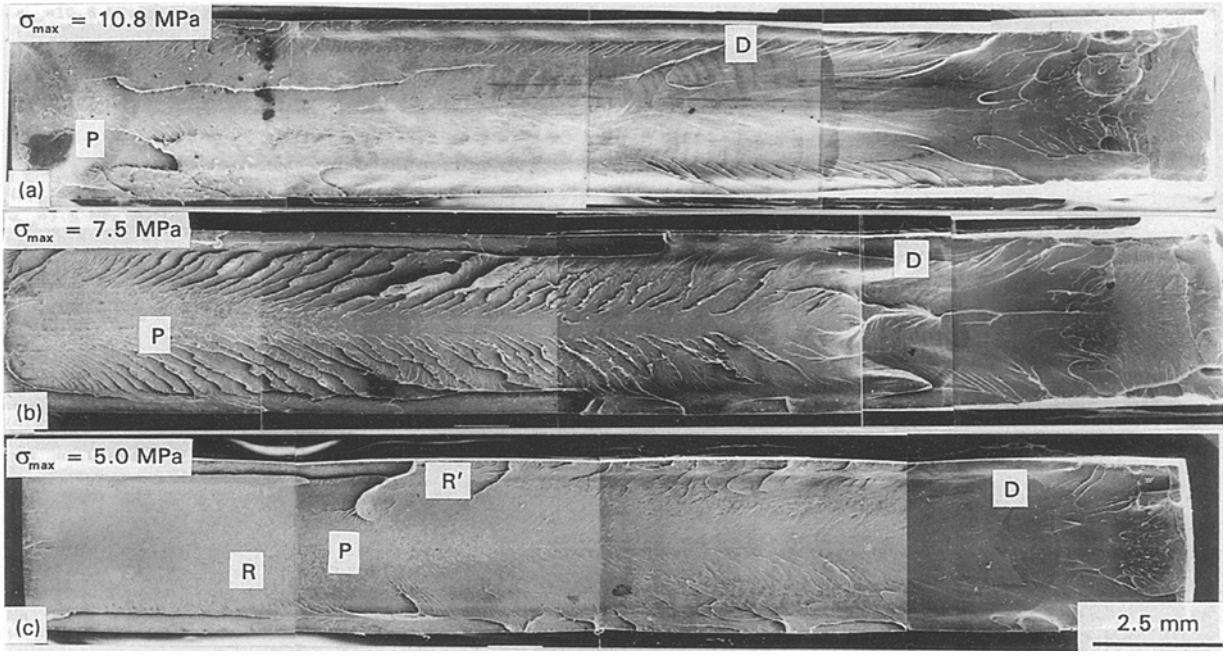

Figure 10 Fracture surfaces of the tests: (a) σ_{max} = 10.8 MPa, (b) σ_{max} = 7.5 MPa, and (c) σ_{max} = 5.0 MPa; (P denotes the patch morphology, D, the fatigue striations, and RR′, a secondary crack).

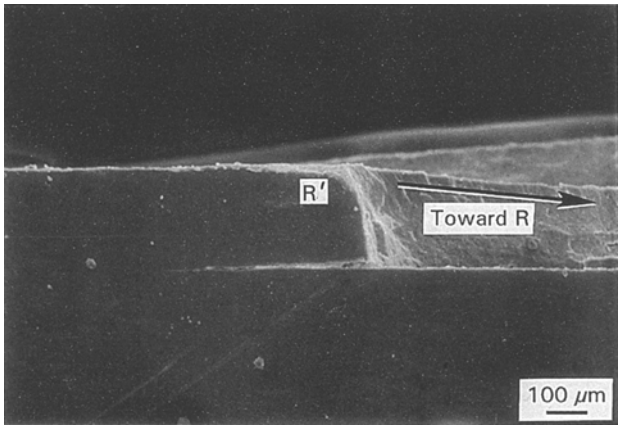

Figure 11 The ridge (R′) as viewed from a direction orthogonal to the fracture surface showing a striking similarity to the ridge of Fig. 5.

difference lines end before reaching the specimen surface. Their curvature indicates that the primary crack overtook the secondary crack before it could reach the specimen surface. By contrast, the $\sigma_{max} = 5.0$ MPa test shows that the RR′ curves become nearly perpendicular to the specimen surface. This is indicative of a faster secondary crack, which could reach the surface to produce the observed ridges. The fact that the test of $\sigma_{max} = 7.5$ MPa shows the most intense crack impingement suggests that their formation is favoured by some optimum balance between stress intensity at the crack tip and the crack speed. It is hypothesized that the load level must be high enough for secondary cracks to initiate, and yet the crack speed must be low enough to allow the secondary crack sufficient time to develop. This presumably explains the relative sparsity of these ridges at the highest and lowest load levels (Fig. 10a and c).

3.3.2. Discontinuous crack growth bands

Since DCG bands have been so closely associated with fatigue, it must be mentioned that they are in fact observed at all the load levels (D). The spacing of fatigue striations indicates the distance traversed by the crack in a given jump. Comparisons with crack speed data have determined that each band is formed in roughly a single loading cycle, thus qualifying them as normal fatigue striations. Such fatigue striations have been reported in ABS [19].

The jumps of the crack have been reported to be slightly smaller than the length of the damage zone [20]. Taking the lowest load level as an example, however, it is found that when the plastic zone length is measured at 2.9 mm, the crack takes jumps that are only about 1% of this, at 30 μm. As the load level increases, the striations comprise successively greater fractions of the damage zone, at 3 and 4%, for damage zones of equivalent length. Because it has been shown that each striation corresponds to crack advance during a single cycle, the striation width is, in this case, equal to the crack speed (frequency 1Hz). In a subsequent paper, we have shown how the irreversible thermodynamics of the damage process can be used to describe the crack speed for both the low and high load levels [2].

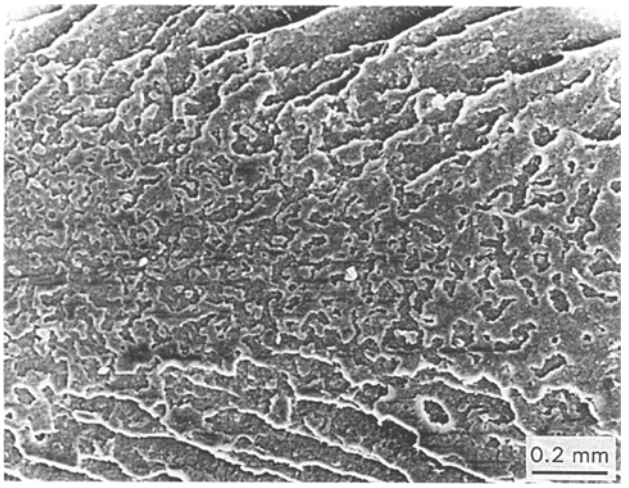

Figure 12 Close-up of the fracture surface patch morphology, $\sigma_{max} = 5.0$ MPa.

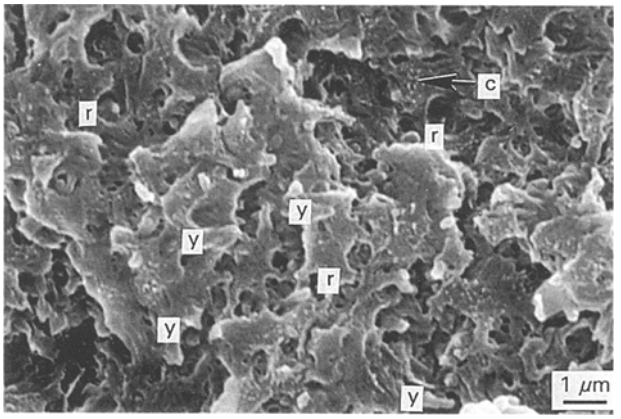

Figure 13 Backbone region of the test $\sigma_{max} = 7.5$ MPa at a crack length of 10 mm showing ruptured rubbery domains (r), local plasticity (y), and craze remnants (C).

3.3.3. Craze features

Just after the initiation region, one notices a patch-like morphology (P) that increasingly pervades the fracture surface with decreasing load level (Fig. 10a–c). A closer view confirms this patch morphology (Fig. 12). This is direct evidence of crack propagation through fully developed crazes on a single plane [20, 21]. It is believed that the stability achieved at lower load levels, and hence lower values of K, permits the crack to propagate in this manner.

Each load level tested shows a distinct transition from the above mentioned patch morphology to a rougher texture. Within this region, the higher magnification permitted by scanning electron microscopy (SEM) reveals voids having sizes in the range of the rubbery domains (Fig. 13). Many of these voids appear to contain the remnants of ruptured rubbery domains (r), reminiscent of similar structures in HIPS and ABS [3, 4]. Surrounding these voids, the matrix appears to have undergone significant yielding, with short, drawn structures extending up from the fracture surface (y). Many of these structures are difficult to discern as they were probably flattened into the plane of the picture by the closure of the crack during the unloading

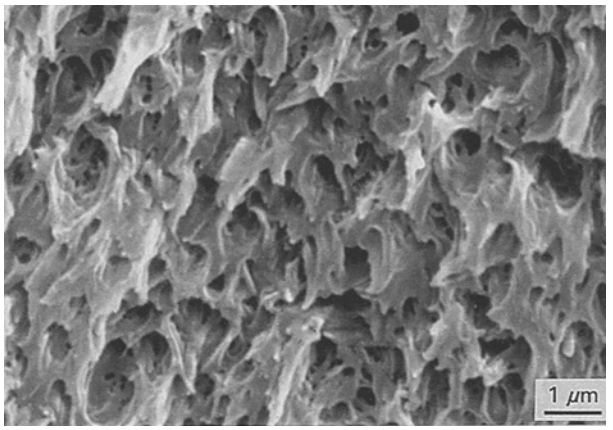

Figure 14 Edge region of the test $\sigma_{max} = 10.8$ MPa at a crack length of about 20 mm showing vacated rubber domain sites and even more extensive local plasticity.

portion of the loading cycle. The thickness of these drawn structures is on the order of 0.5 μm. Since the craze fibrils observed with TEM cannot be any larger than about 11 nm, these are definitely not the same structure. Further, their predominantly flattened, ribbon-like appearance suggests energy dissipating shear tearing of small segments of the matrix. Compatibility of size scale leads one to believe that the crazes discerned by TEM manifest themselves as the tiny white specks (C) seen on the matrix in Fig. 13. Similar features are also attributed to the remnants of broken craze fibrils in HIPS and a rubber-toughened polyphenylene oxide/PS blend [22, 23].

As in the above study [23], it is proposed here that the drawn structures of Fig. 13 are produced in part by the merging of adjacent craze planes by the ductile tearing of the material between them. This, however, cannot be the sole mechanism. Another SEM micrograph taken near the edge of the fracture surface for $\sigma_{max} = 10.8$ MPa and a crack length of about 20 mm shows similar structures (Fig. 14). Yet here, near the side surface, crazes should be minimal, if present at all. This is supported by the absence of the tiny white specks. It is believed that the ribbons are formed as the rubbery domains rupture, thereby transferring load to the surrounding matrix.

4. Conclusions

The mechanism of FCP as a function of load level for an ABS with occluded rubbery domains tested under tension–tension loading was examined. The conclusions are summarized below:

1. At all load levels, the crack tip is preceded by a damage zone containing assemblies of stress-whitened lines that appear to be governed by the maximum principal stress trajectories emanating from the crack tip.
2. Crack growth occurs predominantly through the root stress-whitened line, with occasional jumps into neighbouring lines. These jumps are produced by impingement of secondary internal cracks with the primary crack front, and are most frequent in the medium load level test.
3. Damage within the stress-whitened lines consists of elongated, and occasionally ruptured, rubbery domains at the specimen surface with the appearance of extensive crazes bridging their interstices toward the mid-thickness.
4. The intensity of this crazing (size and number) increases with decreasing load level.
5. The crazes manifest themselves on the fracture surface as a patch morphology, which is increasingly pervasive with decreasing load level.
6. Following the patch morphology, a rougher fracture surface shows evidence of ductile tearing of the matrix. This is believed to be promoted by the rupture of rubbery domains as well as the merging of crazes.
7. Normal fatigue striations show that the crack advances by larger fractions of the damage zone length with increasing load level.

References

1. T. J. BOHATKA and A. MOET, *Exp. Mech.* in press.
2. *Idem., J. Mater. Sci.* in press.
3. J. A. SAUER and C. C. CHEN, *Polym. Eng. Sci* **24** (1984) 794.
4. *Idem. Adv. Polym. Sci.* **52/53** (1983) 217.
5. A. M. DONALD and E. J. KRAMER, *J. Mater. Sci.* **17** (1982) 1765.
6. M. DILLON and M. BEVIS, *ibid.* **17** (1982) 1895.
7. S. L. ROSEN, *Polym. Eng. Sci.* **7** (1967) 115.
8. M. MATSUO, A. UEDA and Y. KONDO, *ibid.* **10** (1970) 1253.
9. H. BREUER, F. HAAF and J. STABENOW, *J. Macromol. Sci. Phys.* **B14** (1977) 387.
10. A. M. DONALD and E. J. KRAMER, *J. Mater. Sci.* **17** (1982) 2351.
11. A. CHUDNOVSKY, K. CHAOUI and A. MOET, *J. Mater. Sci. Lett.* **6** (1987) 1033.
12. D. POST, *Proc. Soc. Exp. Stress Anal.* **12** (1954) 99.
13. M. CHABAAT, *Int. J. Fracture* **37** (1988) R47.
14. R. P. PETRICH, *Polym. Eng. Sci.* **13** (1973) 248.
15. T. J. BOHATKA, M. S. Thesis, Case Western Reserve University, Cleveland, OH (1993).
16. H. BREUER, J. STABENOW and F. HAAF, in Proceedings of the Conference on Toughening of Plastics, London, July 1978, (Plastics and Rubber Institute, London, 1978) Paper 13.
17. R. W. TRUSS and G. A. CHADWICK, *J. Mater. Sci.* **11** (1976) 1391.
18. J. J. STREBEL and A. MOET, *Polym. Eng. Sci.* **33** (1993) 222.
19. A. MISAWA, M. TAKASI and T. KUNIO, 16th Japan Cong. on Mat. Res, **16** (1973) 207.
20. D. HULL, *J. Mater. Sci.* **5** (1970) 357.
21. P. BEAHAN, M. BEVIS, and D. HULL, *Proc. Roy. Soc. Lond.* **A343** (1975) 525.
22. J. A. SAUER and C. C. CHEN, *Adv. Polym. Sci.* **52/53** (1983) 186.
23. T. A. MORELLI and M. T. TAKEMORI, *J. Mater. Sci.* **18** (1983) 1841.

Received 11 April 1994
and accepted 20 January 1995